Fine-tuning the characteristic of the applied potential to improve AC-iEK separations of microparticles

Nuzhet Nihaar Nasir Ahamed,[a] Carlos A. Mendiola-Escobedo,[b] Olivia D. Ernst,[a] Victor H. Perez-Gonzalez[b,*] and Blanca H. Lapizco-Encinas[a,*]

[a] Microscale Bioseparations Laboratory and Biomedical Engineering Department, Rochester Institute of Technology, 160 Lomb Memorial Drive, Rochester, New York, 14623, United States.

[b] School of Engineering and Sciences, Tecnologico de Monterrey, Monterrey, Nuevo Leon 64849, Mexico.

Correspondence should be addressed to the following authors:

Victor H. Perez-Gonzalez (PhD)

Email: vhpg@tec.mx

Blanca H. Lapizco-Encinas (PhD)

Email: bhlbme@rit.edu

ABSTRACT

There is an immediate need for the development of rapid and reliable methods for microparticle and cell assessments, and electrokinetic (EK) phenomena can be exploited to meet that need in a low cost and label-free fashion. The present study combines modeling and experimentation to separate a binary mixture of microparticles of the same size (5.1 μm), shape (spherical), and substrate material (polystyrene), but with a difference in particle zeta potentials of only ~14 mV, by applying direct current (DC)-biased low-frequency alternating current (AC) voltages in an insulator-based-EK (iEK) system. Four distinct separations were carried out to systematically study the effect of fine-tuning each of the three main characteristics of the applied voltage: frequency, amplitude, and DC bias. The results indicate that fine-tuning each parameter improved the separation from an initial separation resolution $R_s = 0.5$, to a final resolution $R_s = 3.1$ of the fully fine-tuned separation. The separation method exhibited fair reproducibility in retention time with variations ranging from 6 to 26% between experimental repetitions. The present study demonstrates the potential to extend the limits of iEK systems coupled with carefully fine-tuned DC-biased low-frequency AC voltages to perform discriminatory micron-sized particle separations.

Keywords:

Alternating Current

Electrokinetics

Electroosmosis

Electrophoresis

Microparticles

INTRODUCTION

An immediate need to develop rapid and reliable techniques for the manipulation, separation, concentration, and isolation of target bioparticles, ranging from macromolecules to parasites, exists in several applications of analytical chemistry. There is a plethora of well-established techniques such as liquid chromatography (LC) and capillary electrophoresis (CE) for the analysis of macromolecules; these methods are well developed and reliable. Both LC and CE can be tailored to target analytes[1] and a suitable mode can be selected from a variety of options.[2] However, the same cannot be said about the availability of well-established methods for the rapid analysis of micron-sized particles such as intact microorganisms and synthetic microparticles of interest.

Microscale electrokinetics (EK) methods offer great potential for the manipulation and analysis of target bioparticles—including not only macromolecules, but nanoparticles and microparticles as well. These methods combine the attractive features of microfluidics (e.g., portability, low cost, and short response time) with the robustness and simplicity of EK phenomena to achieve label-free particle manipulation as function of the electric properties of particles and suspending solution.[3–5] EK-driven microfluidics have been successfully applied for the detection of DNA and proteins,[6–9] enrichment and assessment of cancer cells,[10–13] electrofusion of mammalian cells to create hybrid cells,[14] and separation of microparticles and cells.[15–18]

For micron-sized particles, EK methods are particularly attractive as they offer a rapid culture-free option for the analysis of microorganisms (in contrast to traditional microbe analysis techniques that rely on labor-intensive and time-consuming culture techniques). Therefore, there is great interest in developing microscale EK-based methods for the manipulation and analysis of micron-sized particles, including intact microorganisms. Direct current (DC)-biased CE systems have been used for the assessment and separation of intact microorganisms by some research groups, with the main contributions coming from the Armstrong,[19–23] Buszewski[24–27] and Horká[28–30] labs. Also, conventional DC-iEK-based microsystems have been used by several research groups to separate polystyrene microparticles by exploiting differences of particle zeta potential, ζ_P (i.e., electric charge).[31–36] However, only a few research groups have reported electrokinetic separations using low-frequency (<1 kHz) alternating-current (AC) voltages,[34,35,37,38] which feature up to three control parameters that can be fine-tuned: frequency (f), amplitude, and DC bias—in contrast to conventional DC voltages that only feature a magnitude. So far, for charge-based separation of particles via low-frequency AC signals, the lowest difference in ζ_P is reported to be ~ 40 mV.[34,35] These works, however, did not report a separation resolution R_s.

Recent reports indicate that nonlinear electrophoresis (EP_{NL}) plays a major role in the overall migration of particles in insulator-based systems,[39–41] where the presence of insulating structures distorts the electric field distribution, creating regions of higher field magnitude where nonlinear EK effects can arise.[42–44] This new knowledge increased the potential of EK systems to separate highly similar particles. The separation of almost identical particles (same substrate material, size, shape, and manufacturer), with a difference of only ~4 mV in particle zeta potential, was attempted in a DC-iEK system, obtaining a separation resolution R_s = 1.14, indicating an incomplete or partial separation.[15] Considering the extreme similarity of the particles, this partial separation was encouraging. Additionally, for the first time, the experimental results had a fair agreement with COMSOL predictions.[15,45] In terms of separation of particles by size, our group[36] and several others[46–49] have reported EK-driven separations where target particles differed by several microns in their sizes. Several high-resolution separations of target bioparticles—like closely related microbial strains—have been reported by the Hayes' research group by exploiting the ratio of their EK mobilities.[50–54] Recently, our group also reported a separation involving cells of similar characteristics in an iEK system using a combination of linear and nonlinear electrophoresis.[16] However, all of these separations involved the application of DC voltages to separate the analytes.

On the AC hand, numerous reports exist on the use of electrode-based microsystems—also known as electrode-based dielectrophoresis (eDEP)[55]—and AC fields, where the characteristics of the applied electrical voltages are varied.[10] There are several reports on the use of AC electric fields in iEK systems, where separation mechanisms like absolute negative mobility (ANM),[56] deterministic ANM,[57] and deterministic ratchet migration[58,59] were used to demonstrate size-based separation of micron and submicron sized particles. But there

are very few reports on the use of low-frequency AC voltages in iEK systems.[35,37,47,60,61] Even in these studies, the effect of fine-tuning the different control parameters of the AC input voltage on the separation of similar particles or bioanalytes has not been investigated. Thus, separating microparticles and cells of similar size, shape, and electrical charge by fine-tuning the control parameters of low-frequency AC voltages in iEK systems demands investigation.

The present study addresses this knowledge gap by proposing a novel microscale iEK method that applies DC-biased low-frequency AC voltages to separate microparticles with similar characteristics (size, shape, electrical charge) under the influence of linear and nonlinear EK phenomena. The ultimate goal of this work is to identify a new separation mode in iEK systems where the frequency, amplitude, and offset of the stimulation voltage are fine-tuned to improve the performance of the system, increasing the value of R_s. The present study, focusing on a charge-based separation of microparticles, comprises both, numerical modeling with COMSOL *Multiphysics* and experimentation with iEK microchannels made from PDMS. A binary mixture of polystyrene particles (both featuring 5.1 μm diameter and purchased from the same manufacturer) only differing slightly in particle zeta potential (see **Table 1**) was used to test the potential of our separation approach. A total of four distinct separations were carried out to systematically study the effect of fine-tuning each control parameter of the applied voltage. An electropherogram was obtained after each separation experiment, and the separation performance was assessed in terms of R_s and the number of plates per meter (N/m). COMSOL modeling allowed predicting the retention time ($t_{R,p}$) of each particle type, which was compared with the experimentally obtained retention time ($t_{R,e}$). The deviations between $t_{R,p}$ and $t_{R,e}$ were non-negligible, ranging from -12.1 to 24%. However, the model did not use empirically determined correction factors,[45] and it provided adequate guidance while fine-tuning the control parameters of the system, allowing to improve the separation resolution from an initial value of $R_s = 0.5$ to a final value of $R_s = 3.1$. These results demonstrate the potential of the new proposed approach, illustrating that iEK systems, coupled with carefully fine-tuned AC voltages, have the necessary capabilities to carry out highly discriminatory separations of micron-sized particles.

THEORY

The migration of particles in iEK systems is the result of linear and nonlinear EK forces exerted on the particles. Linear EK phenomena are characterized by velocities that depend linearly on the electric field $\mathbf{E} = E\hat{\mathbf{a}}_E$, where $\hat{\mathbf{a}}_E$ is a unit vector indicating the direction of vector $\mathbf{E}$, which has magnitude E. Linear electrophoresis (EP_L) and linear electroosmotic (EO) flow, with velocities $\mathbf{v}_{EP,L}$ and $\mathbf{v}_{EO}$, respectively, are considered herein:

$$\mathbf{v}_{EP,L} = \mu_{EP,L}\mathbf{E} = \frac{\varepsilon_m \zeta_P}{\eta}\mathbf{E} \tag{1}$$

$$\mathbf{v}_{EO} = \mu_{EO}\mathbf{E} = -\frac{\varepsilon_m \zeta_W}{\eta}\mathbf{E} \quad (2)$$

where $\mu_{EP,L}$ and μ_{EO} are the linear electrophoretic and electroosmotic mobilities, respectively. The suspending medium permittivity and viscosity are represented by ε_m and η, respectively; and ζ_P and ζ_W denote the zeta potential of the particle and the channel wall, respectively. In this study, zeta potential is used as a surrogate for the surface charge density (q_s, **Eq. S1**). Nonlinear EP and dielectrophoresis (DEP) are the nonlinear EK phenomena considered in this study, which feature velocities exhibiting a nonlinear dependence with E**.** The expression for $\mathbf{v}_{DEP}$ exerted on a spherical particle is:

$$\mathbf{v}_{DEP} = \mu_{DEP}\nabla E_{rms}^2 = \frac{r_p^2 \varepsilon_m}{3\eta} Re[f_{CM}]\nabla E_{rms}^2 \quad (3)$$

where $Re[f_{CM}]$ is the real part of the Clausius-Mossotti factor, which describes particle-solution polarization, r_p is the radius of the microparticle, and E_{rms} is the root-mean-square value of the electric field magnitude. Nonlinear EP (EP_{NL}), on the other hand, produces a velocity $\mathbf{v}_{EP,NL}$. Importantly, the mobility of nonlinear EP depends on the electric field magnitude, in contrast to the mobility of EP_L, which is independent of the electric field magnitude.[62] Several models have been developed to describe nonlinear EP. These models rely on the dimensionless Peclet (*Pe*) and Dukhin (*Du*) numbers, and dimensionless applied field strength coefficient (β) to describe the system's conditions and identify the velocity dependence with E (see **Eqns. S2-S4** and **Table S1** in the supplementary material). Analytical expressions for the EP_{NL} velocity ($\mathbf{v}_{EP,NL}$) only exist for the two limiting cases of small *Pe* ($Pe \ll 1$) and high *Pe* ($Pe \gg 1$). No expressions have been developed for the intermediate cases. The expressions of $\mathbf{v}_{EP,NL}$ for the two limiting cases are:[63–65]

$$\mathbf{v}_{EP,NL}^{(3)} = \mu_{EP,NL}^{(3)} E^3 \hat{\mathbf{a}}_E \qquad \text{for arbitrary } Du \text{ and } Pe \ll 1 \quad (4)$$

$$\mathbf{v}_{EP,NL}^{(3/2)} = \mu_{EP,NL}^{(3/2)} E^{3/2} \hat{\mathbf{a}}_E \qquad \text{for } Du \ll 1 \text{ and } Pe \gg 1 \quad (5)$$

where $O(1)$ indicates being comparable in the same first order of magnitude.[65] Considering all four EK phenomena, the expression of the overall particle velocity, $\mathbf{v}_P$, in an iEK device like the one depicted in **Figure 1A** becomes:

$$\mathbf{v}_P = \mathbf{v}_{EO} + \mathbf{v}_{EP,L} + \mathbf{v}_{DEP} + \mathbf{v}_{EP,NL}^{(n)} = \mu_{EO}\,\mathbf{E} + \mu_{EP,L}\,\mathbf{E} + \mu_{DEP}\nabla E^2 + \mu_{EP,NL}^{(n)} E^n \hat{\mathbf{a}}_E \quad (6)$$

where *n* represent the dependence of $\mathbf{v}_{EP,NL}$ with **E** as determined by the operating conditions (see supplementary material **Tables S1-S2**). The operating conditions in the iEK system employed in this study are those listed in **Eq. (4)**, thus, the $\mathbf{v}_{EP,L}$ had the cubic dependence with **E**.

For a binary particle mixture, the parameters of separation resolution (R_s) and number of plates (N) were utilized to assess the quality of each one of the separations carried out in the present study. The expressions for these parameters are illustrated in **Eqns. (7)-(8)**, where W is the width of the peak at the base, $t_{R1,e}$ and $t_{R2,e}$, and W_1 and W_2, are the experimental retention time and width of the peak at the base for particles 1 and 2, respectively.

$$R_s = \frac{2(t_{R2,e} - t_{R1,e})}{W_1 + W_2} \quad (7)$$

$$N = \frac{16 {t_{R,e}}^2}{W^2} \quad (8)$$

The separation occurs by differences in the overall particle velocity, as expressed by **Eq. (6)**. Differences in particle velocity depend on physical properties such as μ_{EO}, $\mu_{EP,L}$, $\mu_{EP,NL}$, μ_{DEP}, ε_m, η, ζ_P, ζ_W and r_p, as shown in **Eqns. (1) to (5)**. The magnitudes of all EK-phenomena also depend on the electric field and, therefore, depend on the position of the particles in the iEK channel and the time at which a measurement is taken, as the electric field distribution is time dependent and non-uniform across the channel. To further understand the physical mechanisms of the different EK phenomena, the reader is referred to the reports by Schnitzer and Yariv.[64,65]

EXPERIMENTAL SECTION

Microdevices. Microdevices were made from polydimethylsiloxane (PDMS, Dow Corning, MI, USA) utilizing standard soft lithography techniques.[37] Microdevices with standard EK injection T-shaped microchannels with circular insulating posts were used.[66] All channels were 40 μm deep and 1.1 mm wide. The dimensions of the posts and channel are detailed in **Figure 1A**.

Suspending medium and microparticles. The suspending medium was a 0.2 mM buffer solution of K_2HPO_4, with the addition of 0.05% (v/v) Tween-20 to prevent clumping of microparticles. The medium had a conductivity of 40.7 μS/cm and a pH of 7.3, which was adjusted by using a 0.1 N KOH solution. Using current monitoring experiments, a wall zeta potential (ζ_W) and μ_{EO} were characterized as -60.1 ± 3.7 mV and ($4.7 \pm$

$0.3)\times 10^{-8}$ m^2 V^{-1} s^{-1}, respectively.[67] Two types of negatively charged 5.1 μm polystyrene microparticles (Magsphere Pasadena, CA, USA) were used at a concentration of 1.2×10^{-8} particles/mL. The values of ζ_P, $\mu_{EP,L}$ and $\mu_{EP,NL}^{(3)}$ were obtained independently for each particle type with particle tracking velocimetry (PTV), as indicated in **Table 1**, by employing a series of low and high voltages in a channel without posts.[39,68] Particles were introduced into the device through EK injection.[66]

Equipment and software. A high-voltage power supply (Model HVS6000D, LabSmith, Livermore, CA) was used to apply electric potentials to the microdevice through four distinct platinum wire electrodes labeled A−D (**Fig. 1A**). Videos of experimental sessions were recorded with a Zeiss Axiovert 40 CFL (Carl Zeiss Microscopy, Thornwood, NY) and a Leica DMi8 (Wetzlar, Germany) inverted microscopes.

Experimental procedure. Prior to experiments, microchannels were filled with the suspending medium 12−16 h before experimentation to ensure a stable EO flow. After introducing the microparticle suspensions (1 μL) into reservoir A (**Fig. 1A**), platinum wire electrodes were placed into the four reservoirs. A standard 3-step EK injection process was utilized by sequentially applying three distinct sets of voltages (i.e., loading, gating, and injection), as shown in **Table 2**.[66,69] Voltages listed in **Table 2** for Separations 2-4 were identified after careful analysis of the numerical predictions produced by our computational model (to be described next), aiming at producing an electropherogram with two well-resolved peaks ($R_s > 1.5$). This is likely to happen when the difference in retention times ($\Delta t_R = t_{R1,p} - t_{R2,p}$) is close to 100 s; smaller Δt_R values might lead to overlapping peaks and larger Δt_R values might lead to lower quality separations. The duration of the last step in each separation was determined by the elution of the microparticles from the channel. The fluorescence signal of each eluting peak was captured at the end of the post array as indicated in the interrogation window of **Figure 1A**. All separations were repeated at least three times to ensure reproducibility (**Table S7**).

Mathematical modeling. COMSOL *Multiphysics* was utilized to build a numerical model of the iEK channel (depicted in **Figure 1A**), which allowed predicting the retention time ($t_{R,p}$) of each particle type in each separation carried out (for details of the models see **Figures S1-S2**, **Tables S2-S6**). To build the model, the microparticles' migration behavior was characterized *a priori* to determine the parameters listed in **Table 1**. To predict the retention time (**Table 3**), the COMSOL model studied the effect of each control parameter (frequency, amplitude, and DC bias) of the applied AC voltage on EK phenomena, enabling fine-tuning of each one of these parameters to design the improved particle separations (see **Tables S3-S6**).

Table 1. Characteristics of the microparticles used in this study, the determination of the mobility of nonlinear electrophoresis was determined in conditions under which the velocity exhibits a cubic dependency with the electric field. This table includes the electric field value used for $\mu_{EP,NL}^{(3)}$ determination consistent with the overall value of the electric field in Separation 1.

ID	Size (μm)	ζ_P (mV)	$\mu_{EP,L}$x10^{-8} (m^{2}V^{-1}s^{-1})	E for $\mu^{(3)}_{EP,NL}$ estimation (V/cm)	$\mu^{(3)}_{EP,NL}$x10^{-17} (m^{4}V^{-3}s^{-1})
Particle 1 - red	5.1	-20.5±2.2	-1.6±0.2	150	-2.5±0.6
Particle 2 - green	5.1	-34.2±3.7	-2.7±0.3	150	-1.6±0.1

Table 2. Voltage conditions employed in each one of the microparticle separations.

ID	Description	Step	Run time (s)	Applied voltage (V) in each reservoir			
				A	B	C	D
1	Non-optimized sinusoidal signal	Loading (DC)	10	1500	900	0	1000
		Gating (DC)	5	2000	2000	200	-100
		Injection (DC)	5	200	500	200	0
		Separation (DC bias + AC)	600	200	350 (DC) + 600 (V_p) @ 0.4 Hz	200	0
2	Frequency optimized signal	Loading (DC)	10	1500	900	0	1000
		Gating (DC)	5	2000	2000	200	-100
		Injection (DC)	5	200	500	200	0
		Separation (DC bias + AC)	600	200	350 (DC) + 600 (V_p) @ 1.1 Hz	200	0
3	Peak amplitude optimized signal	Loading (DC)	10	1500	900	0	1000
		Gating (DC)	5	2000	2000	200	-100
		Injection (DC)	5	200	500	200	0
		Separation (DC bias + AC)	800	200	350 (DC) + 800 (V_p) @ 1.1 Hz	200	0
4	DC bias magnitude optimized signal	Loading (DC)	10	1500	900	0	1000
		Gating (DC)	5	2000	2000	200	-100
		Injection (DC)	5	200	500	200	0
		Separation (DC bias + AC)	800	200	300 (DC) + 800 (V_p) @ 1.1 Hz	200	0

Table 3. Comparison between the COMSOL predicted retention times ($t_{R,p}$) and the experimentally obtained retention times ($t_{R,e}$) for each of the microparticle separations carried out in this study.

Separation ID	R_s	COMSOL predicted $t_{R,p}$ (s)	Experimental $t_{R,e}$ (s)	Deviation $t_{R,p}$ vs. $t_{R,e}$ (%)	Range of deviation in repetitions (%)
1	0.5	182.7	163	-12.1	9-11

		235	297	20.9	7-9
2	1.6	122	162	25	12-16
		235	389	39	18-26
3	2.7	118	128	19.2	10-13
		244	305	7.8	10-13
4	3.1	113	120	-30	6-7
		239	340	22.5	7-9

RESULTS AND DISCUSSION

Microparticle separation employing non-optimized AC signal

To establish a control experiment in this study, we carried out a non-optimized separation of the binary mixture of similar microparticles by simply applying a low-frequency AC electric voltage similar to those reported in our group's previous work.[15,37] Utilizing the suspending medium properties described earlier, the particle properties listed in **Table 1** and **Eqns. (1) to (5)**, the COMSOL model predicted an electrophoretic velocity (linear and nonlinear) antiparallel to the electric field, an electroosmotic velocity parallel to the electric field, and a dielectrophoretic velocity with negligible magnitude as shown in **Figure S4** (consistent with previously reported data[70]). Then, through **Eq. (6)**, the model estimated the impact of the different EK phenomena on particle dynamics and the $t_{R,p}$ values for each particle in a range of applied voltages for the separation step. The experimental results of Separation 1 (input voltages listed in the ID1 row of **Table 2**) are shown in **Figure 1B-C**. **Figure 1B** shows the particles as they migrate across the post array forming "zones", with the 5.1 μm red particles migrating ahead of the green 5.1 μm particles. The electropherogram of this separation is presented in **Figure 1C**, which was built by analyzing the fluorescence signal from the particles as they eluted from the post array. As expected from observing the particle "zones", the red particles eluted first ($t_{R1,e} = 163$ s), followed by the green particles ($t_{R2,e} = 297$ s). This is because red particles have a lower magnitude of ζ_P and $\mu_{EP,L}$ than green ones. The results from three distinct repetitions are reported in **Table S7**, and the deviation between repetitions was in the range of 9 to 11% for the red particles and 7 to 9% for the green particles, respectively. From the electropherogram in **Figure 1C**, the separation resolution was $R_s = 0.5$ (**Eq. 7**), indicating that there is room for improvement in this separation. The number of plates per meter (*N/m,* **Eq. 8**) were $N_1/m = 990$ plates/m and $N_2/m = 1{,}050$ plates/m for red and green particles, respectively. Encouragingly, there is fair agreement between the experimental $t_{R,e}$ and predicted $t_{R,p}$ values, since, as reported in **Table 3**, the deviations between the model and experiments ranged from -12.1 to -35.3 % and from 7.9 to 21% for red and green particles, respectively. The potential causes for these deviations are discussed in detail at the end of the results and discussion section.

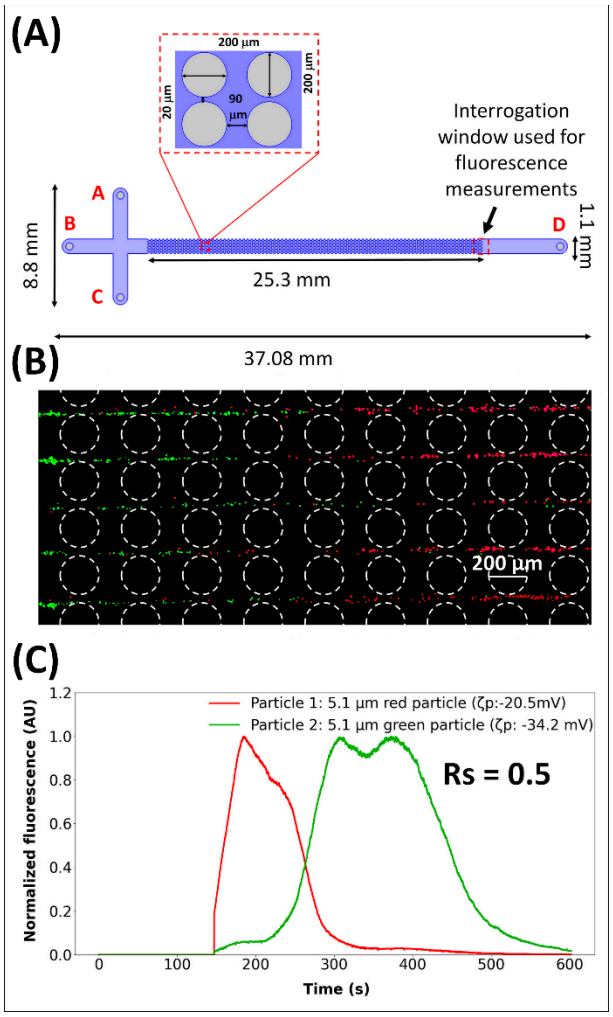

Figure 1. (A) Illustration of the microchannel employed in this work, depicting the dimensions of the channel and insulating posts, as well as the location of the interrogation window used for fluorescence measurements. **(B)** Image of the microparticles beginning to form "zones" within the post array, illustrating the red particles migrating ahead of the green particles (see also Supporting Information Video S1). **(C)** Electropherogram of the microparticle separation built by employing a fluorescence signal obtained at the fluorescence interrogation window. This separation was obtained with a $V_p = 600$ V, at 0.4 Hz and a DC bias of 350 V.

Effect of fine-tuning the frequency of the applied AC signal

The second separation aimed to study the effect of fine-tuning the applied AC signal frequency on the separation of the mixture of similar particles. The numerical model estimated the $t_{R,p}$ values for each particle type in the separation step of the EK injection process for a range of applied frequencies (see **Table S4**). The predicted difference in retention times of both particle types indicated that separation would be possible for the entire range of frequencies evaluated. However, a frequency of 1.1 Hz was selected for experimentation as it exhibited an appropriate difference in retention times as indicated by the dotted red rectangle in **Figure 2A**. Separation 2 was then performed with the voltages listed in row ID2 of **Table 2** at the frequency of 1.1 Hz and results are shown in **Figure 2B-C**. As expected, the red microparticles migrated faster across the array (see **Figure 2B**) as they have a

lower magnitude of ζ_P and $\mu_{EP,L}$. The electropherogram in **Figure 2C** illustrates the peaks obtained from this separation with retention times of $t_{R1,e} = 162$ s and $t_{R2,e} = 389$ s for the red and green particles, respectively and $R_s = 1.6$. This R_s value indicates a significant improvement from Separation 1 ($R_s = 0.5$). These results agree with the study reported by Modarres et al., where successful sorting of microparticles was achieved by tuning the frequency of the applied AC signal.[10] Further, these results support the claim that by tuning the applied AC signal frequency, the R_s of particle mixtures can be improved. This is not to claim that this is the best frequency to be utilized in every AC-based separation, but to provide experimental and numerical evidence that for the chosen set of particles (see **Table 1**), 1.1 Hz was predicted and verified to result in an appropriate difference in retention times, making 1.1 Hz an adequate frequency to proceed with for the next separation experiments. The experimental results had good reproducibility, as deviations between repetitions ranged from 12-16 % and from 18-26% for the red and green particles, respectively (**Table S7**). The efficiencies in terms of *N/m* also illustrate an improvement with $N_1/m = 3{,}374$ plates/m and $N_2/m = 9{,}532$ plates/m for the red and green particles, respectively. There is fair agreement between the experimental ($t_{R,e}$) values and predicted ($t_{R,p}$) values, with $t_{R1,p} = 122$ s and $t_{R2,p} = 235$ s for red and green particles, respectively. The deviation between the computational model and experiments, shown in **Table 3**, were in the range of 21.4 to 39.0% and 12.4 to 39.0% for the red and green particles, respectively. As stated previously, the potential causes for these deviations between the model and the experiments are assessed at the end of the results and discussion section.

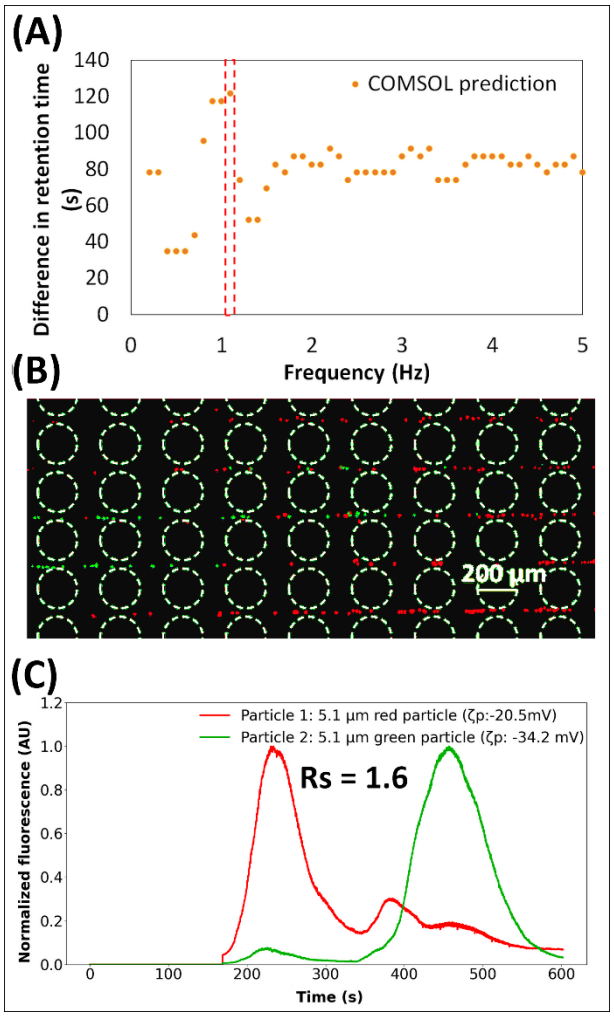

Figure 2. (A) Plot of the predicted retention time versus the frequency of the applied AC signal. The red rectangle indicates the prediction with appropriate difference in retention times. **(B)** Image of the microparticles beginning to form "zones" within the post array, illustrating that the red particles are getting ahead of the green particles (see also Supporting Information Video S2). **(C)** Electropherogram of the microparticle separation built by employing a fluorescence signal obtained at the fluorescence interrogation window. This separation was obtained with a $V_p = 600$ V, at 1.1 Hz and a DC bias of 350 V.

Effect of fine-tuning the peak amplitude of the applied AC signal

The third separation studied the effect of fine-tuning the peak amplitude (V_p) of the applied AC signal at the selected frequency of 1.1 Hz. Based on the $t_{R,p}$ predicted by the COMSOL model (**Table S5**), the microparticle separation was predicted to be feasible with V_p values from 400 to 1150 V. After analyzing the results of COMSOL predictions for different V_p at the fine-tuned frequency (1.1 Hz), the $V_p = 800$ V that resulted in an appropriate difference in retention times (indicated by the dotted red rectangle in **Fig. 3A**) was selected for experimentation. Separation 3 was performed with the voltages listed in row ID3 of **Table 2**, as this combination of voltages should produce well-resolved peaks ($R_s > 1.5$). **Figure 3B** shows an image where the red particles are migrating faster across the insulating post array, which is as expected from their ζ_P and $\mu_{EP,L}$ values. **Figure 3C** shows the

electropherogram from Separation 3, with the red peak eluting at $t_{R1,e} = 128$ s and the green peak eluting at $t_{R2,e} = 305$ s. Importantly, by increasing V_p by 200 V from the 600 V used in Separations 1 and 2, the overall applied electric field magnitude also increases, leading to higher overall particle velocities, and resulting in faster elution as indicated by the $t_{R,p}$ values (**Table 3**). Separation 3 had a resolution of $R_s = 2.7$, indicating both, a complete separation and an improvement in R_s from Separation 2 ($R_s = 1.6$). The efficiencies in terms of *N/m* also improved with $N_1/m = 45{,}869$ plates/m and $N_2/m = 16{,}277$ plates/m for the red and green particles, respectively. Separation 3 had good reproducibility, with deviation between repetitions was in the range of 10 to 13 % for both the red particles and green particles, respectively (**Table S7**). There is fair agreement between the numerical model and experimental results in terms of t_R, with $t_{R1,p} = 118$ s and $t_{R2,p} = 244$ s for red and green particles, respectively, which correspond to deviations in the range of 7.8 to 27% and 20 to 36% for the red and green particles, respectively (**Table 3**). These results demonstrate that for the chosen set of particles, a $V_p = 800$ V, which was predicted to result in the best separation, resulted in a successful experimental separation with significant increase in R_s. This also illustrates the value of numerical models to guide experimentation.

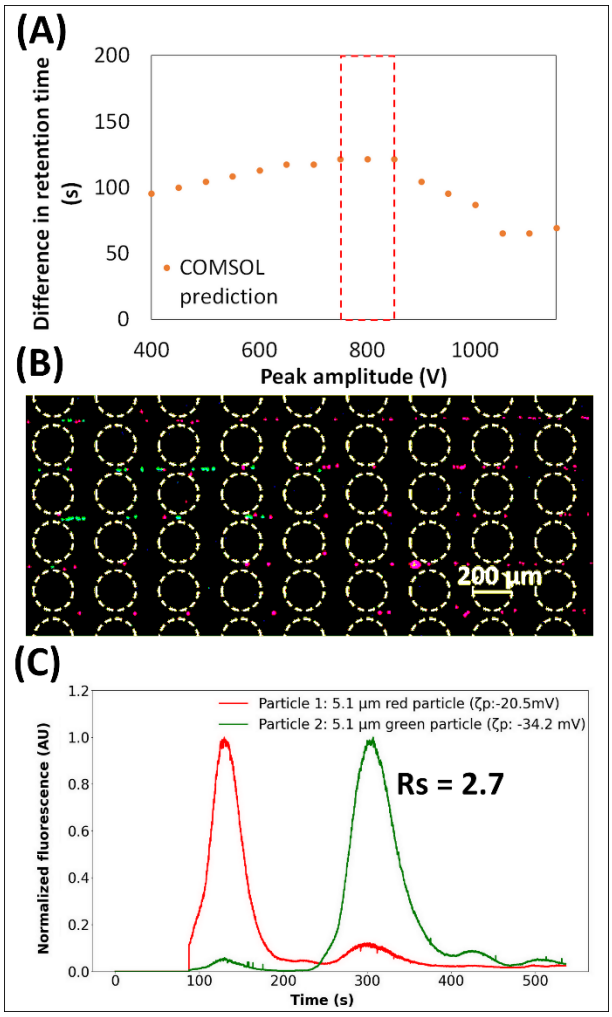

Figure 3. (A) Plot of the predicted retention time versus the peak amplitude of the applied AC signal. The red rectangle indicates the prediction with appropriate difference in retention times. **(B)** Image of the microparticles beginning to form "zones" within the post array, illustrating that the red particles are getting ahead of the green particles. A video of this separation is included as Supporting Information Video S3. **(C)** Electropherogram of the microparticle separation built by employing a fluorescence signal obtained at the fluorescence interrogation window. This separation was obtained with a V_p = 800 V, at 1.1 Hz and a DC bias of 350 V.

Effect of fine-tuning the magnitude of the DC bias of the applied AC signal

The last parameter analyzed in this study was the DC bias of the applied low-frequency AC signal. All previous separations were obtained employing a DC bias of 350 V. A set of COMSOL simulations was carried out employing a V_p = 800 V at 1.1 Hz for a range of distinct DC bias (**Table S6**). The COMSOL predictions illustrated that the appropriate difference in retention times between the particles was obtained for DC bias of 400 and 450 V, as indicated by the dotted red rectangle in **Figure 4A**. Separation 4 was initially performed at a DC bias of 400 V, which did not result in an improvement in R_s (**Fig. S5c**). Tentatively, this can be attributed to the fact that increasing the DC bias results in the applied signal behaving more like a DC signal than an AC signal. As discussed in the sections above, fine-tuning of the AC parameters, frequency and V_p, resulted in improvements of

R_s. To further exploit the advantages provided by the fine-tuned AC signal, Separation 4 was attempted by lowering the magnitude of the DC bias (in spite of numerical predictions indicating that this would reduce the difference in retention times). Nonetheless, as seen in **Figure S5b**, lowering the DC bias too much, resulted in the separation to be too long and thus not desirable due to potential loses in R_s and the appearance of Joule heating effects.[71] However, through these experiments, it was found that a sweet spot exists in DC bias optimization. The sweet spot is neither too low to result in an incomplete separation nor too high to behave like a DC signal and nullify the advantages provided by the AC signal. The combination of voltages and frequency for Separation 4 (**Table 2**) carried out at a DC bias of 300 V, produced significantly improved and well-resolved peaks with $R_s = 3.1$. **Figure 4B** shows the image of the particles across the insulating post array, depicting the red particle migrating ahead, as expected. **Figure 4C** contains the electropherogram of Separation 4 with the red peak eluting at $t_{R1,e} = 120$ s and the green peak eluting at $t_{R2,e} = 320$ s. The value of $R_s = 3.1$ indicates a complete and improved separation when comparing with Separation 3 ($R_s = 2.7$). The efficiency values of Separation 4 in terms of *N/m* were $N_1/m = 7{,}404$ plates/m and $N_2/m = 17{,}512$ plates/m for the red and green particles, respectively, which further illustrate an improvement in the quality of the separation. Excellent reproducibility between experimental repetitions were obtained, with deviation between repetitions in the range of 6 to 7 % and 7 to 9 % for the red and green particles, respectively (**Table S7**). In spite of the discrepancy between predictions and experiments in Separation 4 for the predicted Δt_R values, with $t_{R1,p} = 157$ s and $t_{R2,p} = 248$ s for red and green particles, respectively; resulting in deviations in the range of -16.3 to -30 % and 14.5 to 27 % for the red and green particles, respectively (**Table 3**). As indicated by the model, the appropriate difference in retention times was predicted at 350 and 400 V DC bias, and there is experimental evidence that the quality of resolution obtained in both these conditions is similar ($R_s = 2.7$ and 2.4). It is important to note the gradual improvement in R_s with the optimization of each of the three parameters attributed to the applied AC signal, where R_s improved from 0.5 to 3.1.

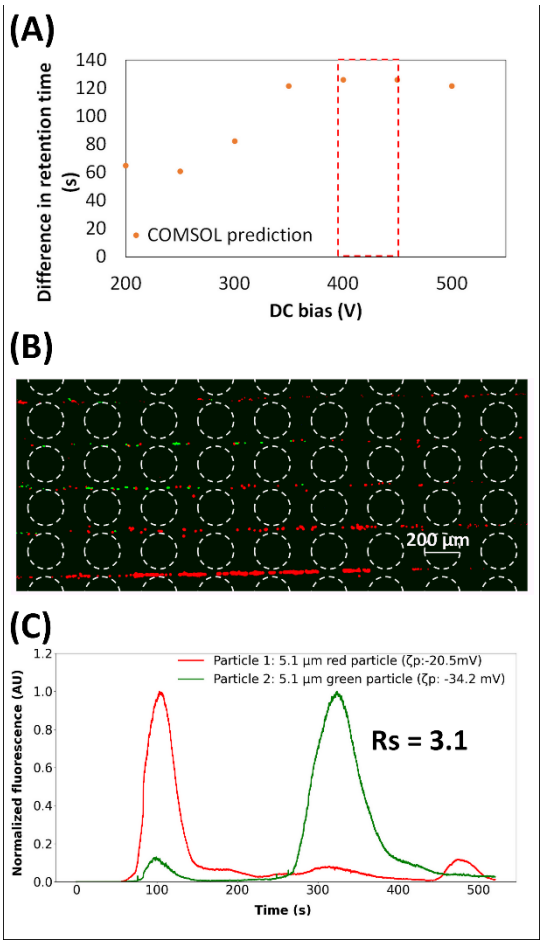

Figure 4. (A) Plot of the predicted retention time versus the DC bias magnitude of the applied AC signal. The red rectangle indicates the prediction with appropriate difference in retention times. **(B)** Image of the microparticles beginning to form "zones" within the post array, illustrating that the red particles are getting ahead of the green particles. A video of this separation is included as Supporting Information **Video S4**. **(C)** Electropherogram of the microparticle separation built by employing a fluorescence signal obtained at the fluorescence interrogation window. This separation was obtained with a $V_p =$ 800 V, at 1.1 Hz and a DC bias of 300 V.

Electrokinetic mechanisms driving the microparticle separation and analysis of model predictions

In all the separations (Separation 1-4), linear EK forces are the main mechanisms responsible to separate the microparticles. As noted in **Table 1**, by closely looking at the properties of the negatively charged microparticles, the values of ζ_P explain these results. The red particles have a lower magnitude of ζ_P and $\mu_{EP,L}$ which means that they experience a lower EP force towards the inlet and have a higher overall velocity ($\mathbf{v}_P$) towards the outlet. This higher velocity allows them to migrate across the entire post array faster than the green particles, as clearly illustrated in the B and C panels of **Figures 1-4**. Based on **Eq. (4)**, care was taken to design each separation in the linear EK regime to avoid dominant nonlinear EP effects since, for this specific set of particles, the magnitudes of the $\mu_{EP}^{(3)}$ mobilities would favor the opposite elution order, *i.e.*, the green particle to be

eluted first, because it has the lower magnitude of $\mu_{EP,NL}^{(3)}$, as noted in **Table 1**. It must be noted, however, that although nonlinear EP effects were not dominant in our experiments they were present and contributed to overall particle behavior. Moreover, for a different set of particles, exploiting nonlinear EP effects for separation purposes might prove beneficial. Hence, the importance of considering nonlinear effects in the numerical model.

To further analyze the relative effect of the each one of the four linear and nonlinear EK phenomena considered here (linear and nonlinear EP, EO flow and DEP), COMSOL simulations were utilized to predict the $\mathbf{v}_P$ and the individual velocities exerted by each EK phenomena on the microparticle migration. These velocity predictions were done over a cutline drawn across one constriction between two insulating posts. The velocity predictions at the maximum value of the x-component of the electric field generated during the application of one cycle of the AC signal, are shown in **Figure S4** for all four separations. **Figures S4A, S4D, S4G, S4J** show one cycle of the applied AC signal where the x-component (dominant at the interrogation point) of the electric field is plotted with respect to time. **Figures S4B-4C, S4E-4F, S4H-4I, S4K-4L** illustrate that the separation was dominated by the two linear EK phenomena: linear EO and EP_L, with a moderate effect of EP_{NL} on the overall velocity of Particle 1, thereby confirming that the linear EK regime favors the selected particle elution order.

Regarding the deviation between modeling and the experimental results observed in Separations 1-4, there are several potential possibilities to explain the cause of deviation. Some viable causes include the effects of electric field distortion caused by the particle themselves, as they are insulating bodies suspended in the media, and dissimilar particle behavior due to particle-particle interactions caused by the relatively high particle concentration.[72] The high particle concentration in the sample plug introduced with EK injection affects the overall particle velocity, as the particles themselves distort the electric field distribution, leading to particle leakage and appearance of shoulders in the electropherograms, as seen in **Figures 1C, 2C, 3C** and **4C**. Another potential cause for the deviations between modeling and experiments, is the effect of "injection bias" in the EK injection process used to introduce the particles into the channel, which would favor the red particles as they have a greater overall migration forward.[69] These potential reasons provide a tentative explanation for why the model underpredicts the $t_{R,p}$ for red particles which are eluted in the presence of green particles, thus accelerating them; and overpredicts the $t_{R,p}$ for green particles, resulting in negative and positive deviations from $t_{R,e}$, respectively. The mathematical model does not currently account for the effects of injections bias and electric field distortion caused by the particle themselves and particle-particle interactions. Considering this, and the fact that no empirical correction factors were employed,[45] the developed COMSOL model is encouraging and useful for designing experimental protocols for challenging particle separations. Though the model developed here is not perfect, it is a valuable tool, with great room for improvement, for constructing and fine-tuning the appropriate parameters of the applied AC signal to obtain efficient resolution in challenging separations.

CONCLUSIONS

This research studied the separation of a binary mixture of similar microparticles, with a small difference in particle zeta potentials of only ~14 mV, by using a new strategy that employs low-frequency AC potentials and the combination of linear and nonlinear EK effects in an iEK microfluidic system. The use of AC potentials allows to fine-tune the characteristics of the applied potential to improve separation resolution, which is an advantage over employing DC potentials. A total of four distinct separations were carried out to systematically investigate the effect of optimizing each of the three main characteristics for the applied AC voltage: frequency, amplitude, and DC bias. Mathematical modeling was performed to select the appropriate conditions for each one of the four separations reported here, and the modeling results, in terms of retention time, were in good agreement with experimental results. The quality of the separations was assessed by employing the parameters of R_s and separation efficiency in terms of *N/m*; showing a gradual improvement from the initial resolution of $R_s = 0.5$, to a final resolution of $R_s = 3.1$ of the fully fine-tuned separation. This is the first report on microparticle separation that considers the effects of nonlinear electrophoresis in a low-frequency AC-iEK and that studies the effect of fine-tuning the different control parameters of an AC input voltage on particle separation. Furthermore, by considering the characteristics of particles (assessed a priori and independently), and the most recent developments in nonlinear electrophoresis, the model predictions allowed identifying the appropriate EK regime (dominant linear or dominant nonlinear) and the required combination of voltages for each separation. The separations results had an adequate reproducibility in terms of $t_{R,e}$ with variations ranging from 6 to 26% between repetitions. This work demonstrates that iEK systems coupled with carefully fine-tuned AC voltages have the capacity to effectively discriminate and separate microparticles of similar characteristics. Also, although the frequency domain of this method is limited to low frequencies and the DC bias can only take values that do not overshadow the superimposed AC signal, together with the amplitude of the AC signal, these control parameters provide a significantly larger number of possible input voltages to exploit for separation purposes than DC-iEK and conventional CE systems do. Future contributions in this field must assess the dynamic range of the technique to determine the maximum and minimum differences in particle zeta potential that the device can reliably handle for particle separation purposes. Also, it will be important to establish the maximum value of the DC-bias that a given input voltage can admit so that the beneficial features of the superimposed AC voltage remain available.

ASSOCIATED CONTENT

Supporting Information

The supplementary file contains **Tables S1-S7** and **Figures S1-S5**. Additionally, the video files Video_S1.mp4, Video_S2.mp4, Video_S3.mp4, and Video_S4.mp4 are also included. These videos depict simultaneously the elution of the microparticles and the plotting of the fluorescence signal as a function of time.

AUTHOR INFORMATION

Nuzhet Nihaar Nasir Ahamed - Microscale Bioseparations Laboratory and Biomedical Engineering Department, Rochester Institute of Technology, Rochester, New York, 14623, United States.

Carlos Alberto Mendiola Escobedo - School of Engineering and Sciences, Tecnologico de Monterrey, Monterrey, Nuevo Leon 64849, Mexico.

Olivia D. Ernst - Microscale BioseparationsLaboratory and Biomedical Engineering Department, Rochester Institute of Technology, Rochester, New York, 14623, United States.

Corresponding Authors

Victor H. Perez-Gonzalez - School of Engineering and Sciences, Tecnologico de Monterrey, Monterrey, Nuevo Leon 64849, Mexico; orcid.org/0000-0003-4503-7774; Email: vhpg@tec.mx

Blanca H. Lapizco-Encinas - Microscale Bioseparations Laboratory and Biomedical Engineering Department, Rochester Institute of Technology, Rochester, New York, 14623, United States; orcid.org/0000-0001-6283-8210; Email: bhlbme@rit.edu

Author Contributions

NNNA: Experimentation, Data Analysis, Writing Original Draft – Review & Editing. **CAME**: Methodology, Data Analysis, Review & Editing. **ODE**: Experimentation, Review of the Paper. **VHPG:** Methodology, Supervision, Writing Original Draft – Review & Editing. **BHLE**: Conceptualization, Methodology, Project administration, Supervision, Writing Original Draft – Review & Editing.

Notes

The authors declare no competing financial interest.

ACKNOWLEDGMENTS

This material is based upon work supported by the National Science Foundation under Award No. 2127592. The authors also acknowledge support from the Kate Gleason College of Engineering, the Nano-Sensors & Devices Research Group (0020209I06) and the Federico Baur Endowed Chair in Nanotechnology (0020240I03) at Tecnologico de Monterrey. The authors also acknowledge the valuable contribution from Alaleh Vaghef-Koodehi for her help in training and experiments.

REFERENCES

(1) Dorsey, J. G. Introduction to Modern Liquid Chromatography, 3rd Ed. *J. Am. Chem. Soc.* **2010**, *132* (26), 9220–9220. https://doi.org/10.1021/ja104156b.

(2) Klepárník, K. Recent Advances in Combination of Capillary Electrophoresis with Mass Spectrometry: Methodology and Theory. *Electrophoresis*. Wiley-VCH Verlag January 1, 2015, pp 159–178. https://doi.org/10.1002/elps.201400392.

(3) Lapizco-Encinas, B. H. Microscale Electrokinetic Assessments of Proteins Employing Insulating Structures. *Curr. Opin. Chem. Eng.* **2020**, *29*, 9–16. https://doi.org/10.1016/J.COCHE.2020.02.007.

(4) Hakim, K. S.; Lapizco-Encinas, B. H. Analysis of Microorganisms with Nonlinear Electrokinetic Microsystems. *Electrophoresis* **2021**, *42* (5), 588–604. https://doi.org/10.1002/elps.202000233.

(5) Sonker, M.; Kim, D.; Egatz-Gomez, A.; Ros, A. Separation Phenomena in Tailored Micro- and Nanofluidic Environments. *Annu. Rev. Anal. Chem.* **2019**, *12* (1), 475–500. https://doi.org/10.1146/annurev-anchem-061417-125758.

(6) Bhatt, G.; Mishra, K.; Ramanathan, G.; Bhattacharya, S. Dielectrophoresis Assisted Impedance Spectroscopy for Detection of Gold-Conjugated Amplified DNA Samples. *Sensors Actuators B Chem.* **2019**, *288*, 442–453. https://doi.org/10.1016/J.SNB.2019.02.081.

(7) Shokouhmand, H.; Abdollahi, A. Detection of Cell-Free DNA Nanoparticles in Insulator Based Dielectrophoresis Systems. *J. Chromatogr. A* **2020**, *1626*, 461262. https://doi.org/10.1016/j.chroma.2020.461262.

(8) Deyanova, E. G.; Huang, R. Y. C.; Madia, P. A.; Nandi, P.; Gudmundsson, O.; Chen, G. Rapid Fingerprinting of a Highly Glycosylated Fusion Protein by Microfluidic Chip-Based Capillary Electrophoresis–Mass Spectrometry. *Electrophoresis* **2021**, *42* (4), 460–464. https://doi.org/10.1002/elps.202000132.

(9) Liu, Y.; Hayes, M. A. Orders-of-Magnitude Larger Force Demonstrated for Dielectrophoresis of Proteins Enabling High-Resolution Separations Based on New Mechanisms. *Anal. Chem.* **2021**, *17*, 21. https://doi.org/10.1021/acs.analchem.0c02763.

(10) Modarres, P.; Tabrizian, M. Frequency Hopping Dielectrophoresis as a New Approach for Microscale Particle and Cell Enrichment. *Sensors Actuators B Chem.* **2019**, *286*, 493–500. https://doi.org/10.1016/J.SNB.2019.01.157.

(11) Çağlayan, Z.; Demircan Yalçın, Y.; Külah, H. Examination of the Dielectrophoretic Spectra of MCF7 Breast Cancer Cells and Leukocytes. *Electrophoresis* **2020**, *41* (5–6), 345–352. https://doi.org/10.1002/elps.201900374.

(12) Dudaie, M.; Nissim, N.; Barnea, I.; Gerling, T.; Duschl, C.; Kirschbaum, M.; Shaked, N. T. Label-Free Discrimination and Selection of Cancer Cells from Blood during Flow Using Holography-Induced Dielectrophoresis. *J. Biophotonics* **2020**, *13* (11). https://doi.org/10.1002/jbio.202000151.

(13) McGrath, J. S.; Honrado, C.; Moore, J. H.; Adair, S. J.; Varhue, W. B.; Salahi, A.; Farmehini, V.;

Goudreau, B. J.; Nagdas, S.; Blais, E. M.; Bauer, T. W.; Swami, N. S. Electrophysiology-Based Stratification of Pancreatic Tumorigenicity by Label-Free Single-Cell Impedance Cytometry. *Anal. Chim. Acta* **2020**, *1101*, 90–98. https://doi.org/10.1016/j.aca.2019.12.033.

(14) Pendharkar, G.; Lu, Y. T.; Chang, C. M.; Lu, M. P.; Liu, C. H. A High Throughput Biocompatible Insulator Based Dielectrophoretic (IDEP) Lab Chip for Patterning and Fusion of Biological Cells. *Sensors Actuators B Chem.* **2022**, *354*, 131109. https://doi.org/10.1016/J.SNB.2021.131109.

(15) Vaghef-Koodehi, A.; Dillis, C.; Lapizco-Encinas, B. H. High-Resolution Charge-Based Electrokinetic Separation of Almost Identical Microparticles. *Anal. Chem.* **2022**, *94* (17), 6451–6456. https://doi.org/10.1021/acs.analchem.2c00355.

(16) Vaghef-Koodehi, A.; Ernst, O. D.; Lapizco-Encinas, B. H. Separation of Cells and Microparticles in Insulator-Based Electrokinetic Systems. *Anal. Chem.* **2023**, *95* (2), 1409–1418. https://doi.org/10.1021/acs.analchem.2c04366.

(17) Bentor, J.; Malekanfard, A.; Raihan, M. K.; Wu, S.; Pan, X.; Song, Y.; Xuan, X. Insulator-Based Dielectrophoretic Focusing and Trapping of Particles in Non-Newtonian Fluids. *Electrophoresis* **2021**, *42* (21–22), 2154–2161. https://doi.org/10.1002/elps.202100005.

(18) Huang, X. H.; Torres-Castro, K.; Varhue, W.; Salahi, A.; Rasin, A.; Honrado, C.; Brown, A.; Guler, J.; Swami, N. S. Self-Aligned Sequential Lateral Field Non-Uniformities over Channel Depth for High Throughput Dielectrophoretic Cell Deflection. *Lab Chip* **2021**, *21* (5), 835–843. https://doi.org/10.1039/d0lc01211d.

(19) Desai, M. J.; Armstrong, D. W. Separation, Identification, and Characterization of Microorganisms by Capillary Electrophoresis. *Microbiol. Mol. Biol. Rev.* **2003**, *67* (1), 38–51. https://doi.org/10.1128/mmbr.67.1.38-51.2003.

(20) Armstrong, D. W.; Schulte, G.; Schneiderheinze, J. M.; Westenberg, D. J. Separating Microbes in the Manner of Molecules. 1. Capillary Electrokinetic Approaches. *Anal. Chem.* **1999**, *71* (24), 5465–5469. https://doi.org/10.1021/ac990779z.

(21) Schneiderheinze, J. M.; Armstrong, D. W.; Schulte, G.; Westenberg, D. J. High Efficiency Separation of Microbial Aggregates Using Capillary Electrophoresis. *FEMS Microbiol. Lett.* **2000**, *189* (1), 39–44.

(22) Girod, M.; Armstrong, D. W. Monitoring the Migration Behavior of Living Microorganisms in Capillary Electrophoresis Using Laser-Induced Fluorescence Detection with a Charge-Coupled Device Imaging System. *Electrophoresis* **2002**, *23* (13), 2048–2056.

(23) Rodriguez, M. A.; Armstrong, D. W. Separation and Analysis of Colloidal/Nano-Particles Including Microorganisms by Capillary Electrophoresis: A Fundamental Review. In *Journal of Chromatography B: Analytical Technologies in the Biomedical and Life Sciences*; Elsevier, 2004; Vol. 800, pp 7–25. https://doi.org/10.1016/j.jchromb.2003.09.060.

(24) Dziubakiewicz, E.; Buszewski, B. Applications of Electromigration Techniques: Electromigration Techniques in Detection of Microorganisms. In *Electromigration Techniques: Theory and Practice*; Buszewski, B., Dziubakiewicz, E., Szumski, M., Eds.; Springer Berlin Heidelberg: Berlin, Heidelberg, 2013; pp 287–298. https://doi.org/10.1007/978-3-642-35043-6_16.

(25) Buszewski, B.; Maślak, E.; Złoch, M.; Railean-Plugaru, V.; Kłodzińska, E.; Pomastowski, P. A New Approach to Identifying Pathogens, with Particular Regard to Viruses, Based on Capillary Electrophoresis and Other Analytical Techniques. *TrAC - Trends Anal. Chem.* **2021**, *139*. https://doi.org/10.1016/J.TRAC.2021.116250.

(26) Rogowska, A.; Pomastowski, P.; Złoch, M.; Railean-Plugaru, V.; Król, A.; Rafińska, K.; Szultka-Młyńska, M.; Buszewski, B. The Influence of Different PH on the Electrophoretic Behaviour of Saccharomyces Cerevisiae Modified by Calcium Ions. *Sci. Rep.* **2018**, *8* (1), 7261. https://doi.org/10.1038/s41598-018-25024-4.

(27) Buszewski, B.; Król, A.; Pomastowski, P.; Railean-Plugaru, V.; Szultka-Młyńska, M. Electrophoretic Determination of Lactococcus Lactis Modified by Zinc Ions. *Chromatographia* **2019**, *82* (1), 347–355. https://doi.org/10.1007/s10337-018-3665-3.

(28) Horká, M.; Karásek, P.; Růžička, F.; Dvořáčková, M.; Sittová, M.; Roth, M. Separation of Methicillin-Resistant from Methicillin-Susceptible Staphylococcus Aureus by Electrophoretic Methods in Fused Silica Capillaries Etched with Supercritical Water. *Anal. Chem.* **2014**, *86* (19), 9701–9708. https://doi.org/10.1021/ac502254f.

(29) Horká, M.; Šalplachta, J.; Karásek, P.; Růžička, F.; Štveráková, D.; Pantůček, R.; Roth, M. Rapid Isolation, Propagation, and Online Analysis of a Small Number of Therapeutic Staphylococcal Bacteriophages from a Complex Matrix. *ACS Infect. Dis.* **2020**, *6* (10), 2745–2755. https://doi.org/10.1021/acsinfecdis.0c00358.

(30) Horká, M.; Štveráková, D.; Šalplachta, J.; Šlais, K.; Šiborová, M.; Růžička, F.; Pantůček, R. Electrophoretic Techniques for Purification, Separation and Detection of Kayvirus with Subsequent Control by Matrix-Assisted Laser Desorption/Ionization Time-of-Flight Mass Spectrometry and Microbiological Methods. *J. Chromatogr. A* **2018**, *1570*, 155–163. https://doi.org/10.1016/j.chroma.2018.07.078.

(31) Jellema, L. C.; Mey, T.; Koster, S.; Verpoorte, E. Charge-Based Particle Separation in Microfluidic Devices Using Combined Hydrodynamic and Electrokinetic Effects. *Lab Chip* **2009**, *9* (13), 1914–1925. https://doi.org/10.1039/b819054b.

(32) Patel, S.; Qian, S.; Xuan, X. Reservoir-Based Dielectrophoresis for Microfluidic Particle Separation by Charge. *Electrophoresis* **2013**, *34* (7), 961–968. https://doi.org/10.1002/elps.201200467.

(33) Zhu, J.; Xuan, X. Curvature-Induced Dielectrophoresis for Continuous Separation of Particles by Charge

in Spiral Microchannels. *Biomicrofluidics* **2011**, *5* (2), 24111. https://doi.org/10.1063/1.3599883.

(34) Calero, V.; Garcia-Sanchez, P.; Ramos, A.; Morgan, H. Combining DC and AC Electric Fields with Deterministic Lateral Displacement for Micro- And Nano-Particle Separation. *Biomicrofluidics* **2019**, *13* (5), 054110. https://doi.org/10.1063/1.5124475.

(35) Lentz, C. J.; Hidalgo-Caballero, S.; Lapizco-Encinas, B. H. Low Frequency Cyclical Potentials for Fine Tuning Insulator-Based Dielectrophoretic Separations. *Biomicrofluidics* **2019**, *13* (4), 044114. https://doi.org/10.1063/1.5115153.

(36) Hill, N.; Lapizco-Encinas, B. H. Continuous Flow Separation of Particles with Insulator-Based Dielectrophoresis Chromatography. *Anal. Bioanal. Chem.* **2020**, *412* (16), 3891–3902. https://doi.org/10.1007/s00216-019-02308-w.

(37) Saucedo-Espinosa, M. A.; Lalonde, A.; Gencoglu, A.; Romero-Creel, M. F.; Dolas, J. R.; Lapizco-Encinas, B. H. Dielectrophoretic Manipulation of Particle Mixtures Employing Asymmetric Insulating Posts. *Electrophoresis* **2016**, *37* (2), 282–290. https://doi.org/10.1002/elps.201500195.

(38) Gencoglu, A.; Olney, D.; Lalonde, A.; Koppula, K. S.; Lapizco-Encinas, B. H. Dynamic Microparticle Manipulation with an Electroosmotic Flow Gradient in Low-Frequency Alternating Current Dielectrophoresis. *Electrophoresis* **2014**, *35* (2–3), 362–373. https://doi.org/10.1002/elps.201300385.

(39) Cardenas-Benitez, B.; Jind, B.; Gallo-Villanueva, R. C.; Martinez-Chapa, S. O.; Lapizco-Encinas, B. H.; Perez-Gonzalez, V. H. Direct Current Electrokinetic Particle Trapping in Insulator-Based Microfluidics: Theory and Experiments. *Anal. Chem.* **2020**, *92* (19), 12871–12879. https://doi.org/10.1021/acs.analchem.0c01303.

(40) Tottori, S.; Misiunas, K.; Keyser, U. F.; Bonthuis, D. J. Nonlinear Electrophoresis of Highly Charged Nonpolarizable Particles. *Phys. Rev. Lett.* **2019**, *123* (1), 14502. https://doi.org/10.1103/PhysRevLett.123.014502.

(41) Bentor, J.; Dort, H.; Chitrao, R. A.; Zhang, Y.; Xuan, X. Nonlinear Electrophoresis of Dielectric Particles in Newtonian Fluids. *Electrophoresis* **2022**, *In press.* (November), 1–9. https://doi.org/10.1002/elps.202200213.

(42) Lapizco-Encinas, B. H. The Latest Advances on Nonlinear Insulator-Based Electrokinetic Microsystems under Direct Current and Low-Frequency Alternating Current Fields: A Review. *Analytical and Bioanalytical Chemistry*. Springer October 19, 2022, pp 885–905. https://doi.org/10.1007/s00216-021-03687-9.

(43) Perez-Gonzalez, V. H. Particle Trapping in Electrically Driven Insulator-Based Microfluidics: Dielectrophoresis and Induced-Charge Electrokinetics. *Electrophoresis* **2021**, *42* (23), 2445–2464. https://doi.org/10.1002/elps.202100123.

(44) Ruz-Cuen, R.; De Los Santos-Ramírez, J. M.; Cardenas-Benitez, B.; Ramírez-Murillo, C. J.; Miller, A.;

Hakim, K.; Lapizco-Encinas, B. H.; Perez-Gonzalez, V. H. Amplification Factor in DC Insulator-Based Electrokinetic Devices: A Theoretical, Numerical, and Experimental Approach to Operation Voltage Reduction for Particle Trapping. *Lab Chip* **2021**, *21* (23), 4596–4607. https://doi.org/10.1039/d1lc00614b.

(45) Hill, N.; Lapizco-Encinas, B. H. On the Use of Correction Factors for the Mathematical Modeling of Insulator Based Dielectrophoretic Devices. *Electrophoresis* **2019**, *40* (18–19), 2541–2552. https://doi.org/10.1002/elps.201900177.

(46) Giesler, J.; Weirauch, L.; Thöming, J.; Baune, M.; Pesch, G. R. Separating Microparticles by Material and Size Using Dielectrophoretic Chromatography with Frequency Modulation. *Sci. Rep.* **2021**, *11* (1), 1–12. https://doi.org/10.1038/s41598-021-95404-w.

(47) Calero, V.; Garcia-Sanchez, P.; Honrado, C.; Ramos, A.; Morgan, H. AC Electrokinetic Biased Deterministic Lateral Displacement for Tunable Particle Separation. *Lab Chip* **2019**, *19* (8), 1386–1396. https://doi.org/10.1039/c8lc01416g.

(48) Yin, D.; Zhang, X.; Han, X.; Yang, J.; Hu, N. Multi-Stage Particle Separation Based on Microstructure Filtration and Dielectrophoresis. *Micromachines* **2019**, *10* (2), 103. https://doi.org/10.3390/mi10020103.

(49) Zhao, K.; Li, D. Continuous Separation of Nanoparticles by Type via Localized DC-Dielectrophoresis Using Asymmetric Nano-Orifice in Pressure-Driven Flow. *Sensors Actuators B Chem.* **2017**, *250*, 274–284. https://doi.org/10.1016/j.snb.2017.04.184.

(50) Liu, Y.; Hayes, M. A. Differential Biophysical Behaviors of Closely Related Strains of Salmonella. *Front. Microbiol.* **2020**, *11* (February), 1–8. https://doi.org/10.3389/fmicb.2020.00302.

(51) Hilton, S. H.; Crowther, C. V.; McLaren, A.; Smithers, J. P.; Hayes, M. A. Biophysical Differentiation of Susceptibility and Chemical Differences in Staphylococcus Aureus. *Analyst* **2020**, *145* (8), 2904–2914. https://doi.org/10.1039/C9AN01449G.

(52) Crowther, C. V.; Hilton, S. H.; Kemp, L. K.; Hayes, M. A. Isolation and Identification of *Listeria Monocytogenes* Utilizing DC Insulator-Based Dielectrophoresis. *Anal. Chim. Acta* **2019**, *1068*, 41–51. https://doi.org/10.1016/j.aca.2019.03.019.

(53) Liu, Y.; Jiang, A.; Kim, E.; Ro, C.; Adams, T.; Flanagan, L. A.; Taylor, T. J.; Hayes, M. A. Identification of Neural Stem and Progenitor Cell Subpopulations Using DC Insulator-Based Dielectrophoresis. *Analyst* **2019**, *144* (13), 4066–4072. https://doi.org/10.1039/c9an00456d.

(54) Jones, P. V.; Huey, S.; Davis, P.; Yanashima, R.; McLemore, R.; McLaren, A.; Hayes, M. A. Biophysical Separation of *Staphylococcus Epidermidis* Strains Based on Antibiotic Resistance. *Analyst* **2015**, *140* (15), 5152–5161. https://doi.org/10.1039/c5an00906e.

(55) Modarres, P.; Tabrizian, M. Alternating Current Dielectrophoresis of Biomacromolecules: The Interplay of Electrokinetic Effects. *Sensors Actuators B Chem.* **2017**, *252*, 391–408.

https://doi.org/10.1016/j.snb.2017.05.144.

(56) Alexandra Ros, Ralf Eichhorn, Jan Regtmeier, Thanh Tu Duong, Peter Reimann, D. A. Absolute Negative Particle Mobility. *Nature* **2005**, *436* (7052), 928. https://doi.org/10.1038/436791a.

(57) Luo, J.; Muratore, K. A.; Arriaga, E. A.; Ros, A. Deterministic Absolute Negative Mobility for Micro- and Submicrometer Particles Induced in a Microfluidic Device. *Anal. Chem.* **2016**, *88* (11), 5920–5927. https://doi.org/10.1021/acs.analchem.6b00837.

(58) Kim, D.; Luo, J.; Arriaga, E. A.; Ros, A. Deterministic Ratchet for Sub-Micrometer (Bio)Particle Separation. *Anal. Chem.* **2018**, *90* (7), 4370–4379. https://doi.org/10.1021/acs.analchem.7b03774.

(59) Ortiz, R.; Koh, D.; Kim, D. H.; Rabbani, M. T.; Anguaya Velasquez, C.; Sonker, M.; Arriaga, E. A.; Ros, A. Continuous Organelle Separation in an Insulator-Based Dielectrophoretic Device. *Electrophoresis* **2022**, *43* (12), 1283–1296. https://doi.org/10.1002/elps.202100326.

(60) Baylon-Cardiel, J. L.; Jesús-Pérez, N. M.; Chávez-Santoscoy, A. V.; Lapizco-Encinas, B. H. Controlled Microparticle Manipulation Employing Low Frequency Alternating Electric Fields in an Array of Insulators. *Lab Chip* **2010**, *10* (23), 3235–3242. https://doi.org/10.1039/c0lc00097c.

(61) Zhang, P.; Liu, Y. DC Biased Low-Frequency Insulating Constriction Dielectrophoresis for Protein Biomolecules Concentration. *Biofabrication* **2017**, *9* (4), 45003. https://doi.org/10.1088/1758-5090/aa82d6.

(62) Khair, A. S. Nonlinear Electrophoresis of Colloidal Particles. *Current Opinion in Colloid and Interface Science*. Elsevier March 25, 2022, p 101587. https://doi.org/10.1016/j.cocis.2022.101587.

(63) Rouhi Youssefi, M.; Diez, F. J. Ultrafast Electrokinetics. *Electrophoresis* **2016**, *37* (5–6), 692–698. https://doi.org/10.1002/elps.201500392.

(64) Schnitzer, O.; Yariv, E. Nonlinear Electrophoresis at Arbitrary Field Strengths: Small-Dukhin-Number Analysis. *Phys. Fluids* **2014**, *26* (12), 122002. https://doi.org/10.1063/1.4902331.

(65) Schnitzer, O.; Zeyde, R.; Yavneh, I.; Yariv, E. Weakly Nonlinear Electrophoresis of a Highly Charged Colloidal Particle. *Phys. Fluids* **2013**, *25* (5), 052004. https://doi.org/10.1063/1.4804672.

(66) Miller, A.; Hill, N.; Hakim, K.; Lapizco-encinas, B. H. Fine-tuning Electrokinetic Injections Considering Nonlinear Electrokinetic Effects in Insulator-based Devices. *Micromachines* **2021**, *12* (6), 628. https://doi.org/10.3390/mi12060628.

(67) Saucedo-Espinosa, M. A.; Lapizco-Encinas, B. H. Refinement of Current Monitoring Methodology for Electroosmotic Flow Assessment under Low Ionic Strength Conditions. *Biomicrofluidics* **2016**, *10* (3), 033104. https://doi.org/10.1063/1.4953183.

(68) Antunez-Vela, S.; Perez-Gonzalez, V. H.; Coll De Peña, A.; Lentz, C. J.; Lapizco-Encinas, B. H. Simultaneous Determination of Linear and Nonlinear Electrophoretic Mobilities of Cells and Microparticles. *Anal. Chem.* **2020**, *92* (22), 14885–14891. https://doi.org/10.1021/acs.analchem.0c03525.

(69) Breadmore, M. C. Electrokinetic and Hydrodynamic Injection: Making the Right Choice for Capillary Electrophoresis. *Bioanalysis*. Future Science Ltd 2009, pp 889–894. https://doi.org/10.4155/bio.09.73.

(70) Coll De Peña, A.; Miller, A.; Lentz, C. J.; Hill, N.; Parthasarathy, A.; Hudson, A. O.; Lapizco-Encinas, B. H. Creation of an Electrokinetic Characterization Library for the Detection and Identification of Biological Cells. *Anal. Bioanal. Chem.* **2020**, *412* (16), 3935–3945. https://doi.org/10.1007/s00216-020-02621-9.

(71) Xuan, X.; Xu, B.; Sinton, D.; Li, D. Electroosmotic Flow with Joule Heating Effects. *Lab Chip* **2004**, *4* (3), 230–236. https://doi.org/10.1039/b315036d.

(72) Saucedo-Espinosa, M. A.; Lapizco-Encinas, B. H. Exploiting Particle Mutual Interactions To Enable Challenging Dielectrophoretic Processes. *Anal. Chem.* **2017**, *89* (16), 8459–8467. https://doi.org/10.1021/acs.analchem.7b02008.

FOR TABLE OF CONTENTS ONLY

Graphical abstract